A Two-Level Prediction Model for Deep Reactive Ion Etch (DRIE)

Hayden K. Taylor, Hongwei Sun, Tyrone F. Hill, Martin A. Schmidt, and Duane S. Boning

Massachusetts Institute of Technology

Abstract **We contribute a quantitative and systematic model to capture etch non-uniformity in deep reactive ion etch of MEMS devices. Non-uniformity depends on uneven distributions of ion and neutral species at the wafer-level, and local consumption at the die-level. An ion-neutral synergism model is constructed from data obtained from several layouts of differing layout pattern densities, and is used to predict wafer-level variation with an r.m.s. error below 3%. This model is combined with a die-level model, which we have reported previously, on a MEMS layout. The two-level model is shown to enable prediction of both within-die and wafer-scale etch rate variation for arbitrary wafer loadings.**

Index Terms **DRIE, pattern dependencies, CAD, modeling.**

I. Introduction

The widespread development of silicon-based MEMS has created a need for MEMS-specific plasma etch technology. Since the etching conditions for high aspect ratio MEMS can result in heavily non-uniform consumption of reactive ion and neutral species, well developed techniques used in the Integrated Circuit (IC) industry such as Reactive Ion Etch (RIE) are not adequate. A plasma etching technique, Deep Reactive Ion Etch (DRIE), has evolved to meet these MEMS requirements. DRIE, which is sometimes referred to as Bosch etching, relies on alternating cycles of ion-assisted chemical etching (SF_6) and polymer deposition (C_4F_8) to achieve parallel sidewalls.

The current literature features several thorough studies of profile control in DRIE [2]–[4]. However, few publications can be found on the modeling of spatial uniformity. Spatial uniformity can be further subdivided into wafer-level and die-level models. Here we focus on the wafer-level model; the die-level model has been presented elsewhere [1]. The model has its origins in ion-neutral synergism, where the contributions from both ions and neutrals are taken into account. This section offers a detailed physical and chemical description of the Bosch process, followed by a presentation of a wafer-level spatial uniformity model. Finally, integration with the die-level model and a comparison with experimental data obtained from a MEMS layout are presented.

A. Bosch Etching

DRIE involves several physical processes including rarified gas flow, gas ionization, ion bombardment, neutral diffusion as well as chemical processes such as neutral-silicon and ion-silicon reactions. A schematic of a typical deep reactive ion etcher (Surface Technology Systems, Newport, Gwent, UK) is shown in Fig. 1.

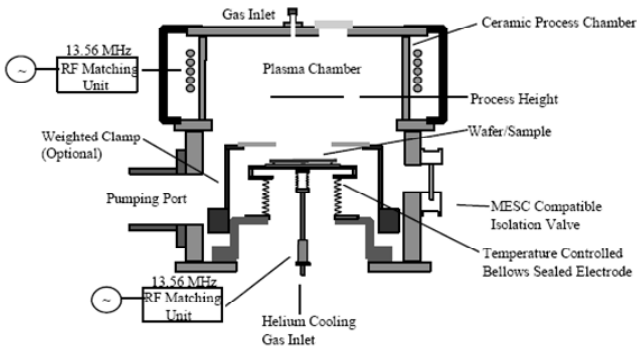

Figure 1: Schematic diagram of an Inductively Coupled Plasma (ICP) deep reactive ion etcher [5].

The tool consists of a 1000 W, 13.5 MHz RF coil, a similar RF matching unit on the wafer backside, a turbopump to achieve low pressures, and an inlet for helium cooling of the wafer from the backside. The gases enter the process chamber from an inlet at the top of the tool; the RF coils are then used to excite the etchant gas into a plasma. After the gases have reacted with the wafer surface, the products are removed from the chamber.

The relevant chemical reactions that occur during Bosch etching are given in simplified form in Eqs. 1 and 2. SF_6 and C_4F_8 are typically used as the etching and passivation gases, respectively. The first equation describes the dissociation of the etchant into ion (S_xF_y) and neutral (F) species. Eq. 2 represents the chemical reaction which results in silicon removal.

$$SF_6 + e^- \longrightarrow S_xF_y + S_xF_y^{\bullet} + F^{\bullet} + e^- \quad (1)$$

$$Si + nF^{\bullet} \longrightarrow SiF_n \quad (2)$$

Manuscript received November 19, 2004.

High aspect ratio directional etching is achieved by alternating between etching and passivation cycles. In the first step, a thin polymeric layer of CF_2 is deposited over a feature. Next, ions accelerated in the plasma sheath remove the polymer from the feature bottom, which is then chemically etched by the fluorine radicals in synergy with energetic ion interactions. Both steps typically range between 5 and 12 seconds in length. Gottscho *et al.* developed an ion–neutral synergism model [6] of the contributions of both ions and neutrals to the etch cycle:

$$\frac{1}{R} = \frac{1}{kE_i J_i} + \frac{1}{vS_o J_n} \tag{3}$$

where R is the etch rate, k and v represent the volume of silicon removed by per unit ion bombardment energy and reacting neutral respectively, J_i and J_n are the ion and neutral fluxes to the surface, E_i is the ion energy, and S_0 is the sticking probability of neutrals to the wafer surface. In general, uniformity depends on several parameters, including ion density, neutral density, and ionic energy at various locations across the wafer, and wafer temperature [7].

In our preliminary work, a wafer-level spatial uniformity map was assumed to be identical to one of a series of etch maps with loading ranging from 0.1% to 17.6%. Loading is defined as the ratio of etchable area to wafer area. The assumption underlying this method is that the wafer-level uniformity will remain approximately the same for nearby values of overall etch loading. For example, a wafer map representing 1.2% loading might be used on a layout with 3% loading. The goal of the new model reported below is to enable intelligent interpolation across the different uniformity maps empirically observed, so that wafer-level uniformity can be accurately predicted for any wafer loading fraction across both ion-dominated and neutral-dominated regimes.

II. Theory and Method

As is outlined in Eq. 3, the ion-neutral synergism model contains contributions from both the ion and neutral fluxes. The ion flux distribution across the wafer depends on asymmetries in the chamber setup; it is believed to be relatively consistent, independent of the overall loading of a layout. Thus, we begin by considering only the neutral distribution across the wafer. An expression for species conservation just above the wafer surface is given in Eq. 4:

$$\frac{\partial C_j}{\partial t} = D\nabla^2 C_j + G_j - R_j \tag{4}$$

where C_j is our species of interest (monatomic fluorine), D is the diffusivity of monatomic fluorine, G_j is the generation rate of monatomic fluorine, and R_j the decay of reactive fluorine into diatomic fluorine (F_2). Several authors have explored analytical and numerical solutions for this differential equation [7]; we are more concerned with empirically modeling its parameters than determining a closed-form solution. In the development of the wafer level model we neglect lateral diffusion across the wafer; thus the diffusive term in eliminated. Lateral interactions between features are addressed by the die-level model. Assuming a steady state situation, we can more explicitly define a relation between the generation and consumption rates:

$$G_j - \alpha_1\left[\varphi + \alpha_2(1-\varphi)\right]C_j - \frac{C_j}{\tau} = 0 \tag{5}$$

Here τ is the average neutral lifetime [s], φ is the proportion of the region in which the silicon is exposed, α_1 is a constant [s^{-1}] for the tool and etch recipe relating the consumption of neutrals to their concentration, and α_2 is a dimensionless constant reflecting neutrals' selectivity of Si over oxide in DRIE. Rearranging Eq. 4 gives

$$C_j = \frac{G_j \tau}{\alpha_1 \tau\left[\varphi + \alpha_2(1-\varphi)\right] + 1} \tag{6}$$

In substituting for the vertical neutral flux, J_n, in the ion-neutral synergism model, we must substitute an expression for the flux at positions where silicon is exposed, rather than an expression for the average flux over exposed and unexposed silicon. Only neutrals that stick to the silicon surface can react, and hence we may write

$$S_0 J_{n,j} = \alpha_1 H\, C_j \tag{7}$$

where S_0 is the sticking probability of neutrals to exposed bare silicon sites, $J_{n,j}$ is the downwards neutral flux just above the wafer at any part of region j that sees exposed silicon, and H is a characteristic height of the dark field above the wafer surface. It is probable that $\alpha_1 H$ will be approximately equal in magnitude to the r.m.s. speed of neutrals in the chamber.

Substituting for $S_0 J_{n,j}$ into the synergism model gives the etch rate R_j for each region as:

$$R_j = \frac{\left(kE_i J_{i,j}\right)\left(v\alpha_1 H G_j \tau\right)}{\left(v\alpha_1 H G_j \tau\right) + \left(kE_i J_{i,j}\right)\left\{\alpha_1 \tau\left[\varphi + \alpha_2(1-\varphi)\right] + 1\right\}} \tag{8}$$

A. Model Extraction and Simulation

We are aiming to predict the silicon etch rate at any position j in the etch chamber for any value of loading, φ. Theory leads to the idea that, in order to make such predictions, we first need to estimate two tool-specific maps: one describing how ion flux varies across the chamber, and another describing how the generation rate of fluorine neutrals varies with position. We also need to estimate the two scalar constants $\alpha_1\tau$ and α_2 to characterize the process.

To obtain enough data to estimate these maps and constants, we etched three wafers with different amounts of

exposed silicon and determined silicon etch rates on those wafers as a function of position. The oxide masking layer on each of three 150 mm-diameter silicon wafers was patterned with a grid of circular openings, the number and diameter of which determined the loading, φ. Wafers were prepared with opening densities of 0.1%, 1.1% and 17.6%. Each wafer was etched in turn for 30 minutes using the following recipe: 105 sccm SF_6 for 14 s at 25 mtorr (100 W platen power and 750 W coil power) interspersed with 40 sccm of C_4F_8 for 11 s at 12 mtorr (60 W platen power and 600 W coil power). On each wafer the depths of 64 of the etched circular holes, on a 16 mm-pitch square grid, were measured interferometrically.

From the data obtained, two 64-point maps and two scalar constants were extracted. In Eq. 9 below, $kE_iJ_{i,j} = A_j$ [ms^{-1}] and $v\alpha_1 HG_j\tau = B_j$ [ms^{-1}]. F is the objective function minimized in order to arrive at our estimates. Each of the 192 test locations, i, on the three characterization wafers corresponds to one of the 64 chamber locations j, and yields a contribution F_i to the objective function:

$$F_i = R_i - \frac{A_j(i)B_j(i)}{B_j(i) + A_j(i)\{\alpha_1\tau[\varphi + \alpha_2(1-\varphi)]+1\}} \quad (9)$$

$$F = \sum_{i=1}^{192} F_i \quad (10)$$

We initially assumed α_2 to be 0.01, reflecting the approximate selectivity of Si over the oxide mask in DRIE. Initial guesses for $\boldsymbol{A}$, $\boldsymbol{B}$ and $\alpha_1\tau$ were calculated by assuming all elements of $\boldsymbol{A}$ and $\boldsymbol{B}$ to be equal. An iterative non-linear least-squares solution of the 192 simultaneous equations given by the experimental data was performed in MatLab. The extracted constants were then used to predict etch rates across a wafer with 4.4% of its surface exposed, and the predictions were compared to measured etch rates from a fourth experimental wafer, featuring 4.4% loading and processed in the manner already described.

III. Results and Discussion

Fig. 2 illustrates etch rate predictions, made using the extracted ion and neutral density maps, next to the corresponding experimental data. Fig. 3 plots measured and predicted etch rates where the horizontal axis corresponds to a "snaking" path around each wafer, as illustrated in Fig. 4. Figs. 2 and 3 confirm that the least-squares fitting procedure has successfully matched our model to the data. In the case of the 4.4% loading previously "unseen" by the model, our approach successfully predicts the way in which etch rates vary across the wafer. As loading increases, an evolution is seen in the form of this variation. At lower loading percentages, we see a "hot spot" of faster etching, while the 17.6% data is defined by a "cold spot" of slower etching. This evolution is illustrated further in Fig. 4. The location of the "hot spot" coincides approximately with the center of the tool's plasma-generating coil. The model does, however, underestimate the magnitude of the etch rates at 4.4% loading, although with a relatively small r.m.s. error of 2.6%.

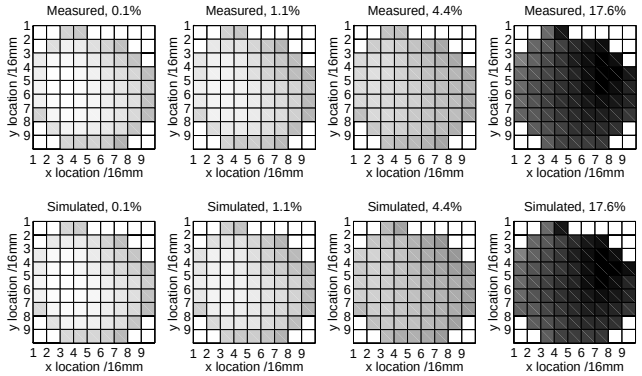

Figure 2: Comparison of experimental and modeled etch rates for four global wafer loadings.

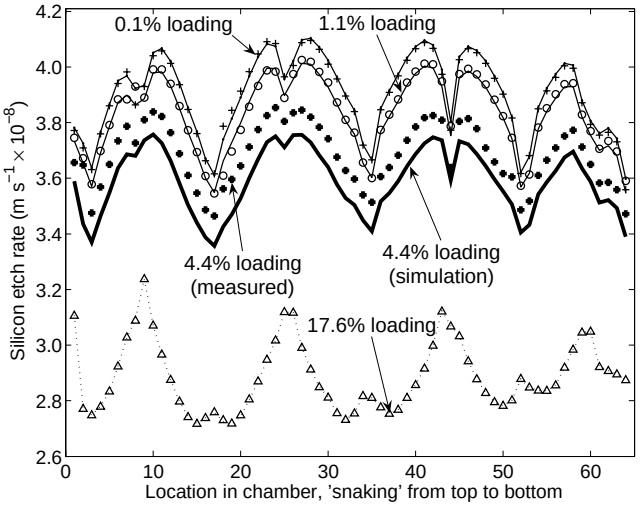

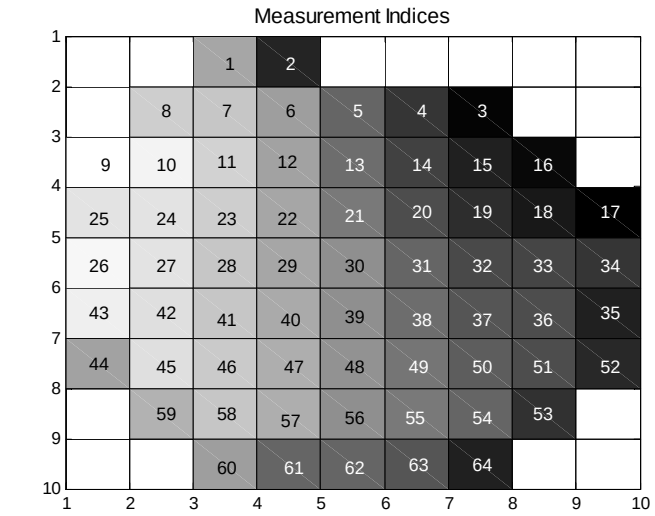

Figure 3: Evolution of etch profile from 0.1% to 17.6% loading, "snaking" from top to bottom. The model was fit to the 0.1%, 1.1%, and 17.6% maps. Measurement indices are given in the lower diagram.

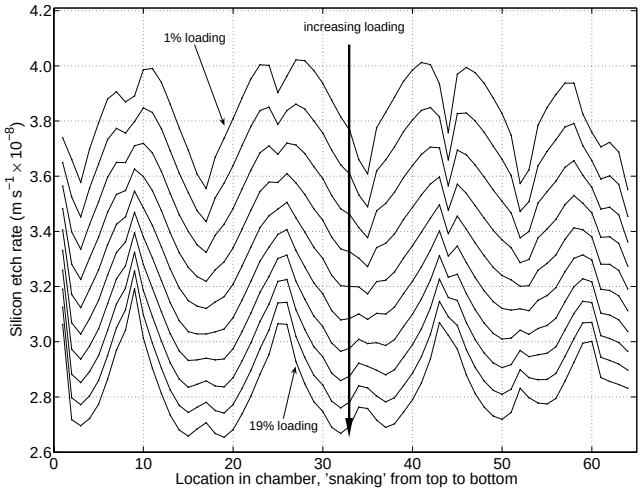

Figure 4: The evolution of wafer-scale etch non-uniformity as the total exposed area of silicon is increased. At 1% loading, the non-uniformity is characterized by a 'hot spot' of particularly rapid etching on the left hand side of the wafer; at 19% loading, the non-uniformity is better described by a 'cold spot' of slower etching on the right. Chamber locations are as given in Fig. 3.

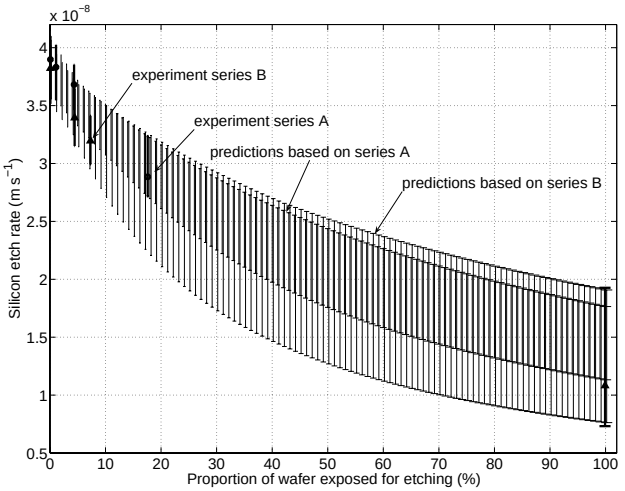

Figure 5: Measured and predicted etch rates as a function of the proportion of the wafer exposed for etching. Both data sets, and the predictions extracted from them, are plotted in this figure. At any given value of loading, a range of etch rates is observed across a wafer. The heights of the vertical bars in this figure indicate the size of that range. The thick vertical bars indicate the measured data; the bands constructed from thin lines indicate predictions of etch rates made using parameters extracted from the measured data.

We have also tested our modeling approach on a second data set, which was obtained in a similar way using the same etching machine a year later. For this second data set, wafers were etched with opening densities of 0.1%, 4.4%, 7.3% and 99.9%. The parameters of our model were fitted to the data obtained at loadings of 0.1%, 4.4% and 99.9%. Data obtained at 7.3% loading were used as an "unseen" set with which to test the model. The interferometric measurements of etch depths made from the wafer with 7.3% loading were on a grid of a different pitch from that of the other data, and so linear interpolation was used to calculate a set of etch rates for easy comparison. Our model, together with the newly extracted parameters, predicted etch rates at 7.3% loading with an r.m.s. error of 4.5%.

Fig. 5 collates all the data obtained and compares etch rate predictions based on data sets A (taken in 2001) and B (taken in 2002). The graph reiterates that as the amount of exposed silicon increases, the average silicon etch rate falls. It is also apparent that as loading increases, the variation of silicon etch rate across the wafer becomes greater.

The etch rate predictions based on data sets A and B are of a similar form, but, for any given loading, data set A implies up to 50% less variation in etch rate across the wafer.

Future work should seek to examine etch rates for loadings between 17.6% and 99.9%, and to investigate the ways in which a particular etching machine's wafer-level non-uniformity changes over time.

A. Combining Predictions with Die-Level Perturbations

Our approach to wafer-scale etch rate variations assumes that each of the wafer locations is equally loaded (*i.e.*, the etching pattern density is uniformly distributed across the surface of the wafer). Central to our ability to model die-to-die effects, however, is the inclusion of the diffusion of reactants parallel to the wafer surface, which thereby results in spatial non-uniformities due to localized differences in the layout pattern density. The new wafer-level model can be combined with our die-level pattern density model to predict uniformity for arbitrary layouts. We assume the relationship between die-level and wafer-level effects is additive; exploration of other coupling mechanisms is ongoing.

We demonstrate the combination of wafer and die-level effects with a compressor blade layout from the MIT microengine project. The layout, shown in Fig. 5, consists of four dies with 42 mm spacing. An image of the layout is given in Fig. 6, while Fig. 7 shows the prediction of normalized etch rate for the lower left die. The measurement was taken at an 8 mm radius from the center, as is indicated by the dashed ring in Fig. 6.

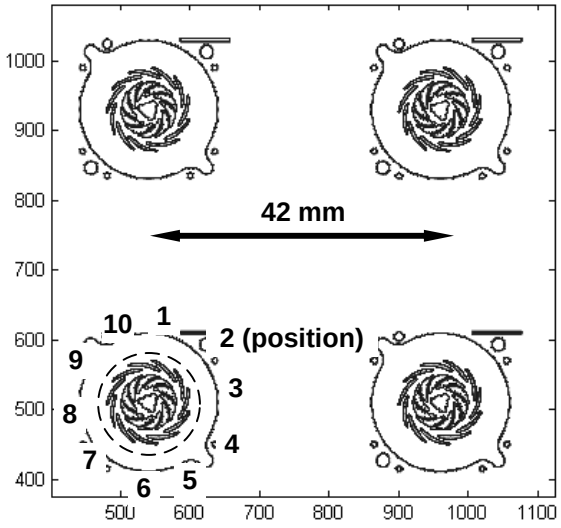

Figure 6: Close-up of compressor die layout; the measurements points are indicated by the dashed ring. The actual layout size is 150 mm × 150 mm.

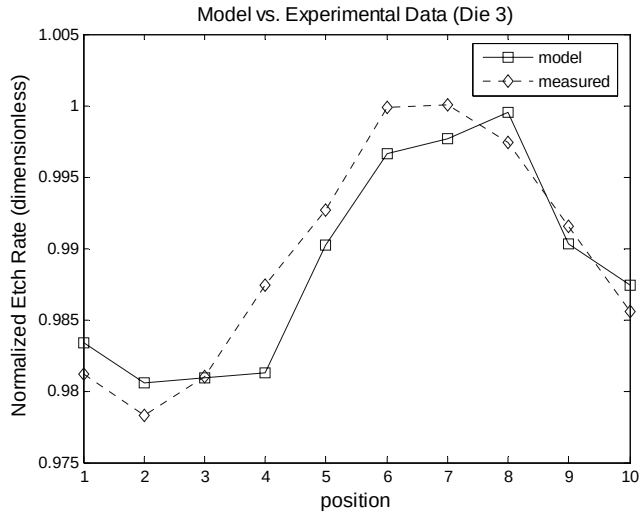

Figure 7: Comparison between model and experimental data for the lower left die in Fig. 4. The agreement indicates that the model is able to accurately capture die-level pattern density effects.

IV. Conclusions

An ion-neutral synergism approach is used to model the wafer-scale non-uniformity in the etching process of DRIE. The model can be extracted from a simple set of wafer-scale etch experiments, enabling identification of both ion and neutral components of spatial non-uniformity. The model can then predict the etch rate uniformity for different wafer loadings. Our model can predict, within less than 3% error on average, the wafer-scale variation of etch rates for an arbitrary amount of exposed silicon on the wafer. Finally, the model was successfully integrated with our pattern density model and demonstrated on a MEMS layout.

V. Acknowledgments

This paper is based on Ref. [16], which is to be presented at MEMS '05 in Miami, FL. This work has been supported in part by the Singapore-MIT Alliance (SMA) and by the Cambridge-MIT Institute (CMI). We also thank Praesagus, Inc. for assistance with layout extractions.

VI. References

[1] T. Hill *et al*., in Tech. Digest of 2002 Hilton Head Solid State Sensors and Actuators Workshop, Hilton Head Island, SC (2004).
[2] A. A. Ayon *et al*., J. of Electrochem. Soc., **146**, 339 (1999).
[3] J. Yeom *et al*., in 12th Int. Conf. On Solid State Sensors, Actuators, and Microsystems, p. 1631, Boston, MA (2003).
[4] J. Kiihamaki *et al*., JVST, A, **18**, 2280 (2000).
[5] J. Bhardwaj *et al*., "Dry Silicon Etching for MEMS," Annual Meeting of the Electrochemical Society, Montreal, Quebec, Canada, May 1997.
[6] R. A. Gottscho *et al*., JVST B, **10**, 2133 (1992).
[7] B. Andersen *et al*., JVST B, **15**(4) (1997).
[8] S. Yun *et al*., J. of App. Phys., **89**, 911 (2001).
[9] J. Karttunen *et al*., Proceedings of SPIE: Micromachining and Microfabrication Process Technology VI, p. 90 (2000).
[10] H. Ashraf *et al*., "Defining Conditions for the etching of silicon in inductive coupled plasma reactor" in 1999 Materials Research Society Fall Meeting, Boston, MA (1999).
[11] H. Sun, T. Hill, M. A. Schmidt, and D. Boning, in 2003 Materials Research Society Fall Meeting, Boston, MA (2003).
[12] S. Shannon, J. Holloway, and M. L. Brake, JVST A, **17**, 2703 (1999).
[13] B.A. Andersen, O. Hansen, and M. Kristensen, JVST B, **15**, 993 (1997).
[14] M. D. Kilgore, H. M. Wu and D. B. Graves, JVST B, **12**, 494 (1994).
[15] A. H. Epstein *et al*., in 28th AIAA Fluid Dynamics Conf., Paper 97–7113 (1997).
[16] H. Sun *et al*., in 18th IEEE Int. Conf. MEMS (2005).